Uncertainty analysis of gamma-ray densitometry applied for gas flow modulation technique in bubble columns

Marchini, S.; Bieberle, A.; Schubert, M.; Hampel, U.;

Originally published:

August 2023

Chemical Engineering Science 282(2023), 119214

DOI: https://doi.org/10.1016/j.ces.2023.119214

Measuring the gas phase dispersion coefficient in bubble columns with the gas flow modulation technique and gamma-ray densitometry: An uncertainty analysis

Sara Marchini[a,b]*, André Bieberle[b], Markus Schubert[b,c]*, Uwe Hampel[a,b]

[a]Chair of Imaging Techniques in Energy and Process Engineering, Technische Universität Dresden, 01062 Dresden, Germany

[b]Institute of Fluid Dynamics, Helmholtz-Zentrum Dresden-Rossendorf, Bautzner Landstraße 400, 01328 Dresden, Germany

[c]Chair of Chemical Engineering, Technische Universität Dresden, 01062 Dresden, Germany

*Corresponding author: s.marchini@tu-dresden.de (S. Marchini)

Abstract

The gas flow modulation technique is a recently proposed approach for measuring the axial gas dispersion coefficient in bubble columns and potentially in other gas-liquid contactors. This study presents a quantitative analysis of the experimental uncertainty that is associated with gamma-ray densitometry and ensemble-averaging of the data. The considered uncertainty sources are the statistics of the photon counting process, a mismatch between the modelled and the real radiation propagation due to the spatial extent of the detector, and a potential mismatch between modulation and sampling frequencies. The analysis is based on a numerical gamma-radiation propagation model and a Monte Carlo approach to account for statistical uncertainty. The proposed algorithm supports the selection of an optimal total scanning time based on detector size, modulation parameters, involved fluids as well as column and source parameters. The analysis reveals that a mismatch between the modulation and sampling frequencies is most critical while the impact of the other considered uncertainty sources is rather marginal.

Keywords

Gas flow modulation technique, axial dispersion coefficient, gamma-ray densitometry, uncertainty analysis

1. Introduction

Hydrodynamics and mass transfer in gas-liquid contactors are most commonly modelled with the one-dimensional axial dispersion model (ADM). It describes the spatiotemporal concentration of a species in the liquid or gas phase via the convection-diffusion equation

$$\frac{\partial c}{\partial t} = D\frac{\partial^2 c}{\partial z^2} - u\frac{\partial c}{\partial z}. \qquad 1$$

Here, c is the concentration of a species in the considered phase, u is the superficial velocity of the considered phase and D is the axial dispersion coefficient. A reliable quantification of the axial liquid and gas dispersion coefficients in gas-liquid contactors is crucial for their design and performance assessment. Recently, Hampel [1] proposed the gas flow modulation (GFM) technique for the non-invasive measurement of the axial gas dispersion coefficient in bubble columns, which is potentially applicable to other gas-liquid contactors as well. Contrary to the traditional approaches based on tracer substances (e.g., [2, 3]), the GFM technique uses a marginal sinusoidal disturbance superimposed on the gas inlet flow rate as virtual tracer. This disturbance introduces a sinusoidal variation of the gas holdup in time, further on referred to as gas holdup wave. Due to the gas dispersion, the gas holdup wave is damped in amplitude and shifted in phase along the column. Mathematically, this can be described in the following way. Assume that the gas flow at the inlet has a constant flow rate plus a marginal sinusoidal change in time. This will produce a modulated gas holdup in the column. Now we consider only the sinusoidal part ϵ' of the gas holdup. At the inlet we may assume it to be of unit strength and zero phase shift, that is $\epsilon'(z = 0, t) = \cos(\omega t)$. Further up the column at a position $z > 0$ we find $\epsilon'(z > 0, t) =$

$V(z)\cos(\omega t + \Delta\varphi(z))$. That is, the gas holdup wave is damped in amplitude (V) and shifted in phase ($\Delta\phi$).

The one-dimensional axial dispersion model for the gas holdup is given in the time domain as

$$\frac{\partial\epsilon(z,t)}{\partial t} = D_{\mathrm{G}}\frac{\partial^2\epsilon(z,t)}{\partial z^2} - u_{\mathrm{G}}^*\frac{\partial\epsilon(z,t)}{\partial z}, \qquad 2$$

and in the frequency domain as

$$\mathrm{j}\omega E(z,\omega) = D_{\mathrm{G}}\frac{\partial^2 E(z,\omega)}{\partial z^2} - u_{\mathrm{G}}^*\frac{\partial E(z,\omega)}{\partial z}, \qquad 3$$

where z is the axial distance from the gas sparger, D_{G} is the axial gas dispersion coefficient, u_{G}^* is the average bubble rise velocity, $\omega = 2\pi f$ is the modulation frequency and E is the time-domain Fourier transform of the axial gas holdup distribution. Solving Equation 3 analytically one can derive the following expressions for V and $\Delta\phi$ between two axial planes with distance Δz [1]:

$$V = \exp\left(\frac{u_{\mathrm{G}}^*}{2D_{\mathrm{G}}}\left[1 - \frac{1}{\sqrt{2}}\sqrt{1 + \sqrt{1 + \frac{16\omega^2 D_{\mathrm{G}}^2}{{u_{\mathrm{G}}^*}^4}}}\right]\Delta z\right), \qquad 4$$

$$\Delta\phi = -\frac{u_{\mathrm{G}}^*}{D_{\mathrm{G}}\sqrt{8}}\left[\sqrt{\left[\sqrt{1 + \frac{16\omega^2 D_{\mathrm{G}}^2}{{u_{\mathrm{G}}^*}^4}}\right] - 1}\right]\Delta z. \qquad 5$$

Both equations are needed for determining the axial gas dispersion coefficient. In fact, the limited sensitivity of Equation 5 to a change in D_{G} does not allow reliable calculation of D_{G}, as shown by Marchini et al. [4]. In addition, multiple solutions to Equation 4 in terms of D_{G} exist in at least part of the domain. In order to use Equations 4 and 5 for calculating D_{G} the values of the amplitude and phase of the gas holdup wave must be measured at least at two axial positions in the column. This was first demonstrated by Döß et al. [5] using gamma-ray densitometry as illustrated in the simplified scheme in **Figure 1a**.

Recently, Marchini et al. [4] introduced a theoretical analysis and quantification of the inherent uncertainty caused by the use of the axial dispersion model for describing the gas holdup wave.

However, this comprehensive analysis did not take into account the contribution of the experimental uncertainty to the measured amplitude attenuation and phase shift. Thus, the objective of this paper is to fill this gap.

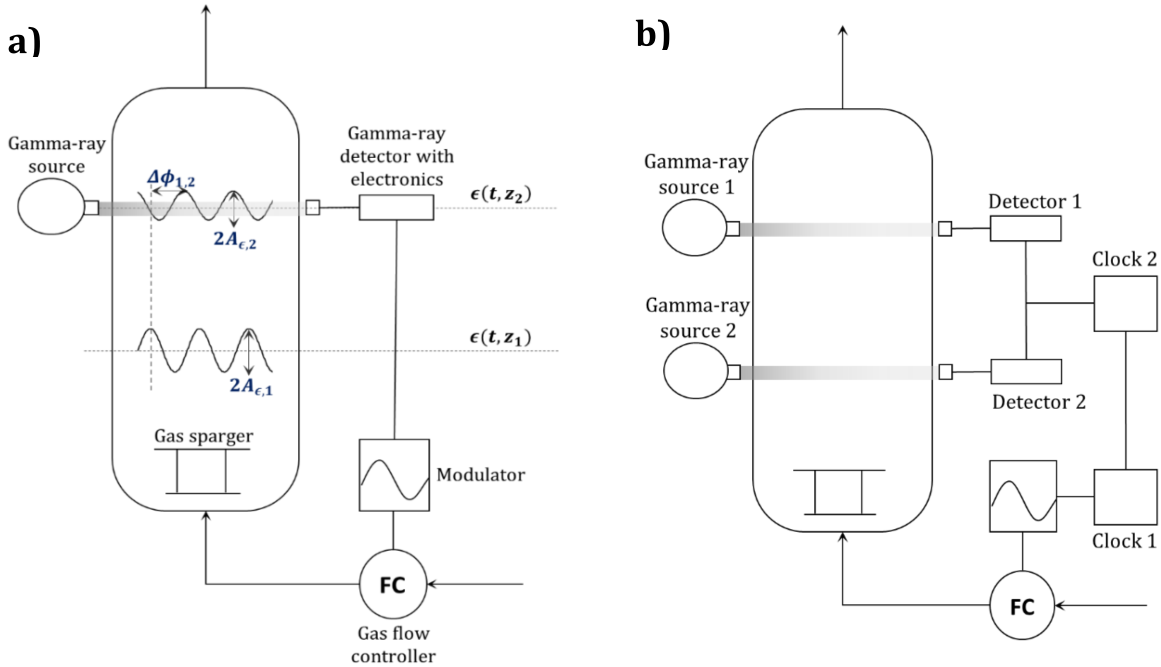

Figure 1. Simplified scheme of the experimental setup needed for axial gas dispersion coefficient measurement using gamma-ray densitometry with (a) one or (b) two synchronized detector elements and radiative sources.

An alternative arrangement to the one represented in **Figure 1a** is composed of two radiative sources and two detector elements. The detectors sample simultaneously at two different axial positions of the column and are synchronized with the same clock (Clock 2). The gas flow modulator, instead, relies on another clock (Clock 1). Both clocks are again synchronized with each other. This configuration allows measuring at the same time at both axial positions, reducing the impact of possible deviations in the process and the time needed to perform the measurements. A representative scheme is provided in **Figure 1b**.

In both configurations, the parameters contributing to experimental uncertainty are manifold and dependent on the specific setup. This work considers uncertainty sources that are common to most gamma-ray densitometry setups, i.e. statistics of the photon counting process, a mismatch between the modelled and the real radiation propagation due to the spatial extent of the detector, and a potential mismatch between modulation and sampling frequencies. In this study, numerical experiments are preferred over real ones due to the high number of repetitions needed for each experiment. Furthermore, such a numerical approach enables to decouple the above-mentioned uncertainty sources that act together in real experiments.

The proposed approach is used to simulate the gamma-photons registered by a gamma-ray detector to quantify the impact of the selected uncertainty sources depending on the operating conditions as well as on column characteristics. The algorithm also supports optimizing the scanning time and sampling frequency for cost-efficient experiments.

2. Ensemble-averaging gamma-ray densitometry and uncertainty sources

Gamma-ray densitometry is based on the measurement of the linear attenuation of radiation within an object. Therefore, an isotopic source and a photon-counting detector are arranged opposite to each other at the object of interest such that radiation from the source passes the object and is registered by the detector. The detector counts single photons arriving from the source. Hence, in the following we denote by N the number of photons being registered in a given time interval ΔT. In case of a gas-liquid contactor, we find the following relationship for radiation attenuation:

$$\langle N_{\mathrm{GL}} \rangle = \langle N_{\mathrm{G}} \rangle \exp(-\mu_{\mathrm{L}} l (1 - \epsilon)). \tag{6}$$

Here, $\langle N_{\mathrm{GL}} \rangle$ is the expected number of photons registered per time interval for an operating contactor (note, that subscript G stands for gas and L stands for liquid), $\langle N_{\mathrm{G}} \rangle$ is the expected number of photons one would register per time interval for the contactor containing no liquid. Furthermore, μ_{L} is the linear attenuation coefficient of the liquid, l is the total length of the process space the radiation beam passes and ϵ is the gas holdup within the beam path. Here, two technical remarks are necessary. First, the derivation of Equation 6 assumes that the linear attenuation coefficient of the gas phase $\mu_{\mathrm{G}} = 0$. For contactors operating at very high pressures we may have $\mu_{\mathrm{G}} > 0$, but this can be considered in a straightforward way. Second, in gamma-ray densitometry the detector will inevitably record some additional natural radiation in addition to the radiation from the isotopic source. It is therefore assumed that this constant offset is known and corrected.

Every radiation-emission-detection process is associated with a statistical uncertainty. The count number in a time interval fluctuates and the statistical distribution of the count number is described by a Poisson distribution

$$P(N) = \frac{\langle N \rangle^N}{N!} \exp(-\langle N \rangle), \quad (7)$$

where $P(N)$ is the probability of detecting N photons if $\langle N \rangle$ are expected. Note, that $N \in \mathbb{N}$ and $\langle N \rangle \in \mathbb{R}$.

To reduce the impact of the statistics of the photon counting process on measured amplitude and phase, Döß et al. [5] applied a lock-in detection scheme, that synchronises the detector data acquisition with the gas flow modulation. The detection events were then ensemble-averaged by counting them within $n_{\mathrm{s}} = f_{\mathrm{s}}/f$ equidistant scanning intervals, where f_{s} and f are the sampling and modulation frequencies, respectively. **Figure 2** illustrates this schematically. From here on, ensemble-averaged data are indicated with a tilde.

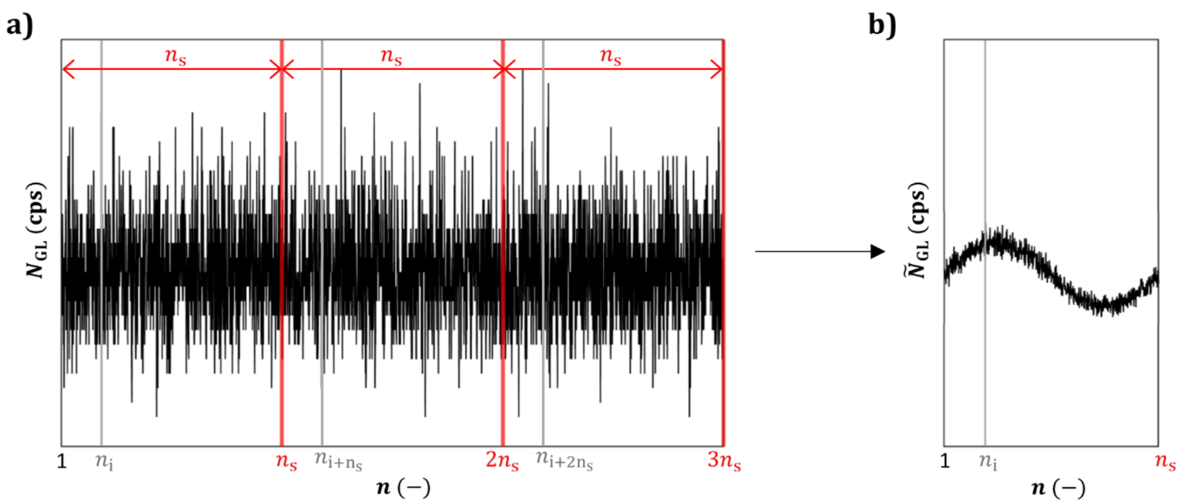

Figure 2. Schematic of the ensemble-averaging procedure, in which (a) the original detector data stream is subdivided into single modulation periods that are (b) subsequently averaged to reduce statistical noise. This way, the modified modulation wave is obtained.

As a result, one obtains the ensemble-averaged count number distributions for one modulation period containing n_s values. This distribution is logarithmized to obtain gas holdup data. A cosine function is then fitted to the resulting data, whose amplitude and phase are determined by a least-squares criterion. Note that if there was no logarithmization one could also do a Fourier analysis to obtain amplitude and phase.

Using gamma-ray densitometry one needs to consider its specific sources of uncertainty. First, the gamma-ray detector is commonly assumed to be point-like. However, in reality, the extent of the detector is a source of uncertainty. In case of a circular object (i.e. a column), the penetration length changes along the detector width while the gas holdup wave changes its amplitude and phase along the detector height. Another uncertainty source addressed in this study is a mismatch between the modulation and sampling frequencies and vice versa. This may be due to insufficiently synchronized clocks. Any mismatch between the modulation and sampling frequencies reduces the reliability of the reconstructed amplitude and phase.

3. Methodology

In this section, we present an approach that predicts the gamma-photon rate registered by the detector at a certain axial position. At a fixed axial position, the gas holdup for the sinusoidal modulation is a function of time, that is

$$\epsilon(t) = \bar{\epsilon} + A_\epsilon \cos(\omega t + \phi), \qquad 8$$

where $\bar{\epsilon}$ is the time-averaged gas holdup, A_ϵ is the modulation amplitude, and ϕ is the modulation phase. Substituting Equation 8 in Equation 6, the expected number of counts in time for given amplitude and phase of the gas holdup wave is

$$\langle N_{\mathrm{GL}}(t)\rangle = \langle N_{\mathrm{G}}\rangle \exp(-\mu_{\mathrm{L}}(1-\bar{\epsilon}-A_{\epsilon}\cos(\omega t+\phi))l)\,. \tag{9}$$

Equation 9 is used to model gamma-ray densitometry for assumed modulation parameters ($\bar{\epsilon}$, A_{ϵ}, ϕ, ω), initial count number (N_{G}), column geometry (l) and working fluids (μ_{L}). Count numbers are simulated for n_{tot} equal-size time intervals between $t = 0$ and $t = t_{\mathrm{tot}}$. For each time interval we compute a count number realization N_{GL} by drawing a Poisson-distributed number (Equation 7) using the expectation value computed from Equation 9. Having done so for all n_{tot} sampling points we perform the ensemble averaging and logarithmization which gives the gas holdup distribution for one ensemble-averaged period as

$$\tilde{\epsilon}_{\mathrm{i}}^{*} = \frac{1}{\mu_{\mathrm{L}} l}\log\left(\frac{\widetilde{N}_{\mathrm{GL,i}}}{\langle N_{\mathrm{G}}\rangle}\right) + 1\,. \tag{10}$$

Eventually, these data are then fitted by a cosine function as

$$\epsilon^{*}(t) = \bar{\epsilon}^{*} + A_{\epsilon}^{*}\cos(\omega t + \phi^{*}), \tag{11}$$

obtaining the amplitude A_{ϵ}^{*} and phase ϕ^{*}. The comparison between A_{ϵ}^{*} and A_{ϵ} and between ϕ^{*} and ϕ provides a quantification of the uncertainty caused by the statistics of the photon counting process on amplitude damping and phase shift, respectively.

Since the fitting of the cosine function is only based on the specific values of $\boldsymbol{\widetilde{N}_{\mathrm{GL}}}$, several repetitions of the same experiment are necessary to obtain a reliable assessment, as typical for Monte Carlo approaches. The results obtained this way offer more than 95% confidence level. It should be noted that the deviation caused by statistics of the photon counting process is physically inherent to all configurations and setups.

The detector size plays a role for the statistics of the photon counting process and further the spatial extent of the detector may have the consequence that radiation attenuation does no longer fit to a simple one-beam model. The count rate increases with the extension of the detector. Considering an empty process space, the number of detection events in a time interval ΔT is given by

$$\langle N_{\mathrm{G}} \rangle = \frac{\Phi S \Delta T}{4\pi L^2}, \tag{12}$$

where Φ is the gamma-radiation flux of the source (photon emission rate into the full solid angle of 4π sr) and S is the detector area. The geometrical parameters are illustrated in **Figure 3**. A bigger detector improves the statistics (since it increases $\langle N_{\mathrm{G}} \rangle$). However, an increased detector size results in changes in the real object length accompanied by changes in the gamma-ray attenuation along the horizontal direction (detector width $L_{\mathrm{d,y}}$). Additionally, the detector height $L_{\mathrm{d,z}}$ affects the measurement since the amplitude and phase of the gas holdup wave change along the vertical axis of the contactor.

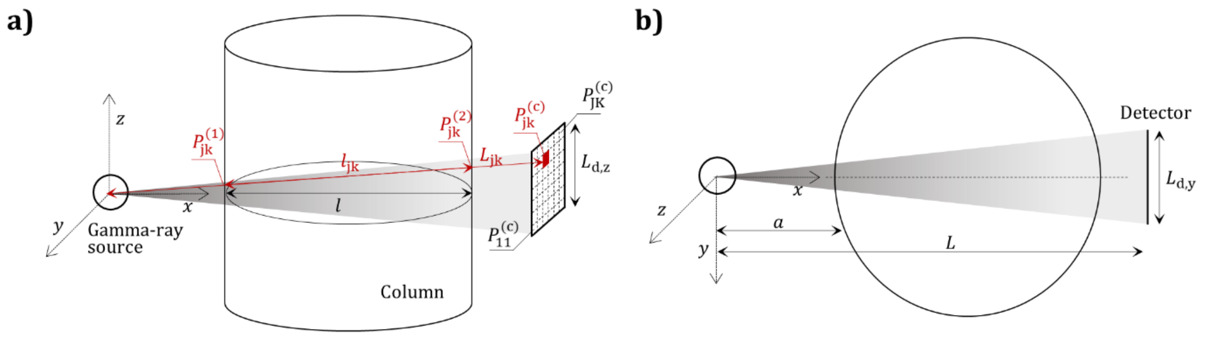

Figure 3. Symbols used in Section 5 (parameters used describing a single detector element is labelled in red) and illustration of the effect of the detector height (a) and width (b).

4. Statistical uncertainty in the photon counting process

In this section, we assess the uncertainty in amplitude and phase caused by the statistics of the photon counting process. For this purpose, the detector is assumed small enough so that the penetration length is constant and equal to the length of the beam in the process space. Here, amplitude and phase do not change within the axial limits of the detector. The effect of the detector size will be analysed in Section 5. Considering a measurement time t_{tot} and a sampling frequency f_{s}, the total expected number of counts for each interval t_{i} of the modulation period (i.e., here $0 \leq t_{\mathrm{i}} \leq 1/f$) is (see Equations 9 and 12)

$$\langle N_{\mathrm{GL,i}} \rangle = \frac{t_{\mathrm{tot}} f}{f_{\mathrm{s}}} \langle N_{\mathrm{G}} \rangle \exp(-\mu_{\mathrm{L}} l (1 - \epsilon_{\mathrm{i}})). \tag{13}$$

Defining

$$K_1 = \frac{t_{\mathrm{tot}} f}{f_{\mathrm{s}}} \langle N_{\mathrm{G}} \rangle \exp\left(K_2 \left(1 - \frac{1}{\bar{\epsilon}} \right) \right), \tag{14}$$

$$K_2 = \mu_{\mathrm{L}} \bar{\epsilon} l \,, \tag{15}$$

Equation 13 can be rewritten as

$$\langle N_{\mathrm{GL,i}} \rangle = K_1 \exp(K_2 A \cos(\omega t_{\mathrm{i}} + \phi)), \tag{16}$$

where K_1 and K_2 are independent of the considered time interval. The above-presented algorithm is used to evaluate the effect of K_1 and K_2 on the standard deviations in amplitude damping and phase-shift, which are reported in **Figure 4** and defined as

$$\mathrm{Dev}A = \frac{1}{A} \sqrt{\frac{1}{e} \sum_{\mathrm{i}=1}^{e} (A_{\mathrm{i}}^{*} - A)^2}, \tag{17}$$

$$\mathrm{Dev}\phi = \frac{1}{\phi} \sqrt{\frac{1}{e} \sum_{\mathrm{i}=1}^{e} (\phi_{\mathrm{i}}^{*} - \phi)^2}, \tag{18}$$

where A and ϕ are the expected values of amplitude and phase, while A_{i}^{*} and ϕ_{i}^{*} are amplitude and phase obtained from each numerical experiment. The number of repetition for each experiment is indicated as e.

Table 1 gives values of K_1 and K_2 for typical configurations and working fluids. An analysis of the effect of A and ϕ, for constant values of K_1 and K_2 is reported in the **Supplementary Material S1**. This analysis showed that the phase of the gas holdup has only a limited effect on the uncertainty on the phase itself. On the contrary, a higher amplitude substantially reduces the uncertainty of both in terms of amplitude and phase. However, as discussed by Marchini et al. [4], the initial modulation amplitude should be kept below 15% to avoid an effect of the modulation on the hydrodynamics of the column.

Table 1. Examples of obtained K_1 and K_2 for different configurations.

<table>
<tr><th>Case N.
(−)</th><th>$\mu_L l$
(−)</th><th>$\langle N_G \rangle$
(cps)</th><th>$t_{tot} f f_s^{-1}$
(s)</th><th>$\bar{\epsilon}$
(−)</th><th>K_1
(s^{-1})</th><th>K_2
(−)</th></tr>
<tr><td>1</td><td rowspan="6">5</td><td>$4.9 \cdot 10^3$</td><td rowspan="6">14.4</td><td rowspan="6">0.1</td><td>783</td><td rowspan="6">0.5</td></tr>
<tr><td>2</td><td>$9.8 \cdot 10^3$</td><td>1566</td></tr>
<tr><td>3</td><td>$2.7 \cdot 10^4$</td><td>4349</td></tr>
<tr><td>4</td><td>$6.1 \cdot 10^4$</td><td>9785</td></tr>
<tr><td>5</td><td>$1.3 \cdot 10^5$</td><td>19569</td></tr>
<tr><td>6</td><td>$1.5 \cdot 10^5$</td><td>24462</td></tr>
<tr><td>7</td><td rowspan="6">1</td><td>$1.3 \cdot 10^3$</td><td rowspan="2">1.7</td><td rowspan="6">0.15</td><td>941</td><td rowspan="6">0.15</td></tr>
<tr><td>8</td><td rowspan="3">$2.5 \cdot 10^3$</td><td>1882</td></tr>
<tr><td>9</td><td>3.5</td><td>3764</td></tr>
<tr><td>10</td><td rowspan="2">7.0</td><td>7529</td></tr>
<tr><td>11</td><td rowspan="2">$4.9 \cdot 10^3$</td><td>15058</td></tr>
<tr><td>12</td><td>14.4</td><td>30117</td></tr>
<tr><td>13</td><td rowspan="6">1</td><td>$1.3 \cdot 10^3$</td><td rowspan="2">1.7</td><td rowspan="6">0.1</td><td>895</td><td rowspan="6">0.10</td></tr>
<tr><td>14</td><td rowspan="3">$2.5 \cdot 10^3$</td><td>1790</td></tr>
<tr><td>15</td><td>3.5</td><td>3581</td></tr>
<tr><td>16</td><td rowspan="2">7.0</td><td>7162</td></tr>
<tr><td>17</td><td rowspan="2">$4.9 \cdot 10^3$</td><td>14324</td></tr>
<tr><td>18</td><td>14.4</td><td>28648</td></tr>
</table>

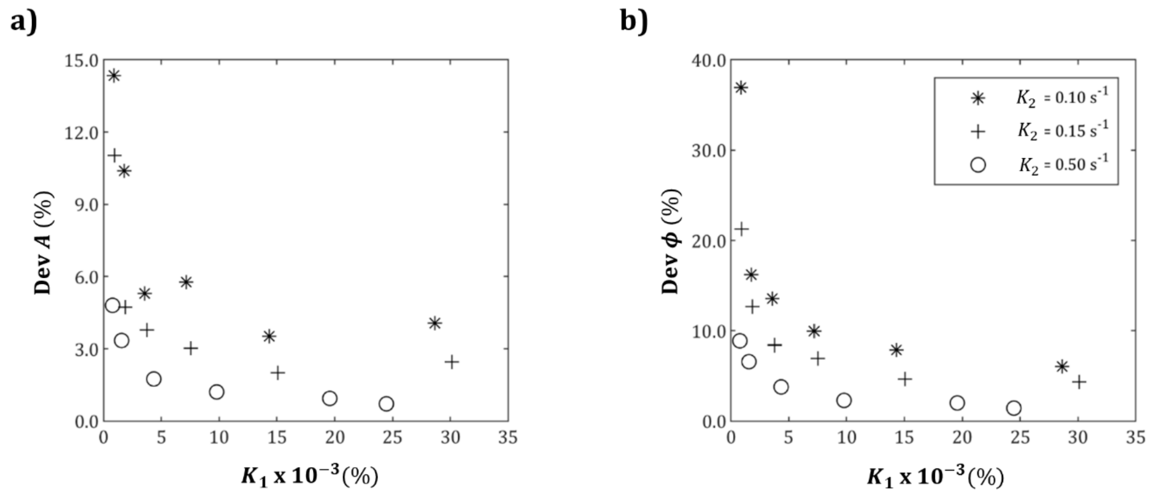

Figure 4. Deviation of amplitude and phase as a function of K_1 and for different values of K_2 ($A = 0.15, \phi = 0.5$).

Figure 4 shows a decrease in both deviations increasing K_1 and K_2. However, it should be noted that K_1 itself is dependent on K_2 and it decreases significantly when the latter is increased.

5. Effect of the spatial extent of the detector

As pointed out in Section 4, the detector size influences the value of K_1. In particular, a larger detector can be used to increase the photon count rate and, therefore, reduce the deviation in amplitude and phase. However, the changes along the detector surface in the length of the radiation beam inside of the process space and in the gas holdup were not considered. In this section, the impact of these assumptions is quantified in terms of additional uncertainty, neglecting the effect of the statistics of the photon counting process.

The problem is approached dividing the detector into a number of small rectangular sections with columns (index j) and rows (index k) and center coordinates $P_{\mathrm{jk}}^{(\mathrm{c})}\left(x_{\mathrm{jk}}^{(\mathrm{c})}, y_{\mathrm{jk}}^{(\mathrm{c})}, z_{\mathrm{jk}}^{(\mathrm{c})}\right)$ as shown in **Figure 3a**. Accordingly, each detector section contributes with

$$N_{\mathrm{GL,jk}} = N_{\mathrm{G,jk}} \exp\left(-(1-\bar{\epsilon})\mu_{\mathrm{L}} L_{\mathrm{jk}}\right) \exp\left(A_{\epsilon,0}\mu_{\mathrm{L}} \int_0^{l_{\mathrm{jk}}} V(l') \cos\left(\omega t + \Delta\phi(l')\right) \mathrm{d}l'\right). \qquad 19$$

If the ray penetrates and leaves the column (considered as an empty cylindrical process space) in $P_{\mathrm{jk}}^{(1)}(x_{\mathrm{jk}}^{(1)}, y_{\mathrm{jk}}^{(1)}, z_{\mathrm{jk}}^{(1)})$ and $P_{\mathrm{jk}}^{(2)}(\mathrm{x}_{\mathrm{ji}}^{(2)}, y_{\mathrm{ji}}^{(2)}, z_{\mathrm{ji}}^{(2)})$, respectively, the penetration length is

$$l_{\mathrm{jk}} = \sqrt{\left(x_{\mathrm{jk}}^{(2)} - x_{\mathrm{jk}}^{(1)}\right)^2 + \left(y_{\mathrm{jk}}^{(2)} - y_{\mathrm{jk}}^{(1)}\right)^2 + \left(z_{\mathrm{jk}}^{(2)} - z_{\mathrm{jk}}^{(1)}\right)^2}. \tag{20}$$

The total number of counts reaching the detector is given by the sum of the counts reaching each section, that is

$$\begin{aligned} N_{\mathrm{GL}} = F \sum_{\mathrm{k}=1}^{\mathrm{K}} \sum_{\mathrm{j}=1}^{\mathrm{J}} \frac{1}{L_{\mathrm{jk}}^2} \exp\left(-(1-\bar{\epsilon})\mu_{\mathrm{L}} l_{\mathrm{jk}}\right) \\ \cdot \exp\left(A_{\epsilon,0}\mu_{\mathrm{L}} C \int_{z_{\mathrm{jk}}^{(1)}}^{z_{\mathrm{jk}}^{(2)}} \exp(H_1 z)\cos(\omega t + \mathrm{H}_2 z + \phi_0)\,\mathrm{d}z\right), \end{aligned} \tag{21}$$

where

$$F = \frac{\Phi S}{4\pi f_{\mathrm{s}}} \tag{22}$$

$$H_1 = \frac{u_{\mathrm{G}}^*}{2D_{\mathrm{G}}}\left[1 - \frac{1}{\sqrt{2}}\sqrt{1 + \sqrt{1 + \frac{16\omega^2 D_{\mathrm{G}}^2}{{u_{\mathrm{G}}^*}^4}}}\right], \tag{23}$$

$$\mathrm{H}_2 = -\frac{u_{\mathrm{G}}^*}{D_{\mathrm{G}}\sqrt{8}}\left[\sqrt{\left[\sqrt{1 + \frac{16\omega^2 D_{\mathrm{G}}^2}{{u_{\mathrm{G}}^*}^4}}\right] - 1}\right], \tag{24}$$

$$C = \sqrt{1 + \left(\frac{x_{\mathrm{jk}}^{(2)} - x_{\mathrm{jk}}^{(1)}}{z_{\mathrm{jk}}^{(2)} - z_{\mathrm{jk}}^{(1)}}\right)^2 + \left(\frac{y_{\mathrm{jk}}^{(2)} - y_{\mathrm{jk}}^{(1)}}{z_{\mathrm{jk}}^{(2)} - z_{\mathrm{jk}}^{(1)}}\right)^2} \tag{25}$$

and

$$L_{\mathrm{jk}} = \sqrt{{x_{\mathrm{jk}}^{(\mathrm{c})}}^2 + {y_{\mathrm{jk}}^{(\mathrm{c})}}^2 + {z_{\mathrm{jk}}^{(\mathrm{c})}}^2}. \tag{26}$$

The detailed derivation of Equation 21 is given in the **Supplementary Material S2**.

Equation 21 was solved numerically for given values of $F/S, H_1, H_2, A_{\epsilon,0}\mu_{\mathrm{L}}$ and for a given relative position between the column and the measurement system. The solution was obtained for different normalized values of the detector width and height ($L_{\mathrm{d,y}}/l$ and $L_{\mathrm{d,z}}/l$ in **Figure 5**) and for each time step t_{i} considering a single modulation period. The obtained number of counts was then converted into holdup data as

$$\epsilon_{\mathrm{i}}^* = 1 + \frac{1}{\mu_{\mathrm{L}} l} \ln\left(\frac{L^2 N_{\mathrm{GL,i}}}{F}\right) = \bar{\epsilon}^*(1 + A^* \cos(\omega t_i + \phi^*)) \tag{27}$$

and fitted by a cosine function. The obtained amplitude, phase and average holdup are then compared with their expected values $\bar{\epsilon}$, $\phi = H_2 z + \phi_0$ and $A = A_{\epsilon,0} \exp(H_1 z)$. **Figure 5** reports the obtained results for

$$\mathrm{Dev}A = \frac{A^* - A}{A}, \tag{28}$$

$$\mathrm{Dev}\phi = \frac{\phi^* - \phi}{\phi}, \tag{29}$$

$$\mathrm{Dev}\bar{\epsilon} = \frac{\bar{\epsilon}^* - \bar{\epsilon}}{\bar{\epsilon}}. \tag{30}$$

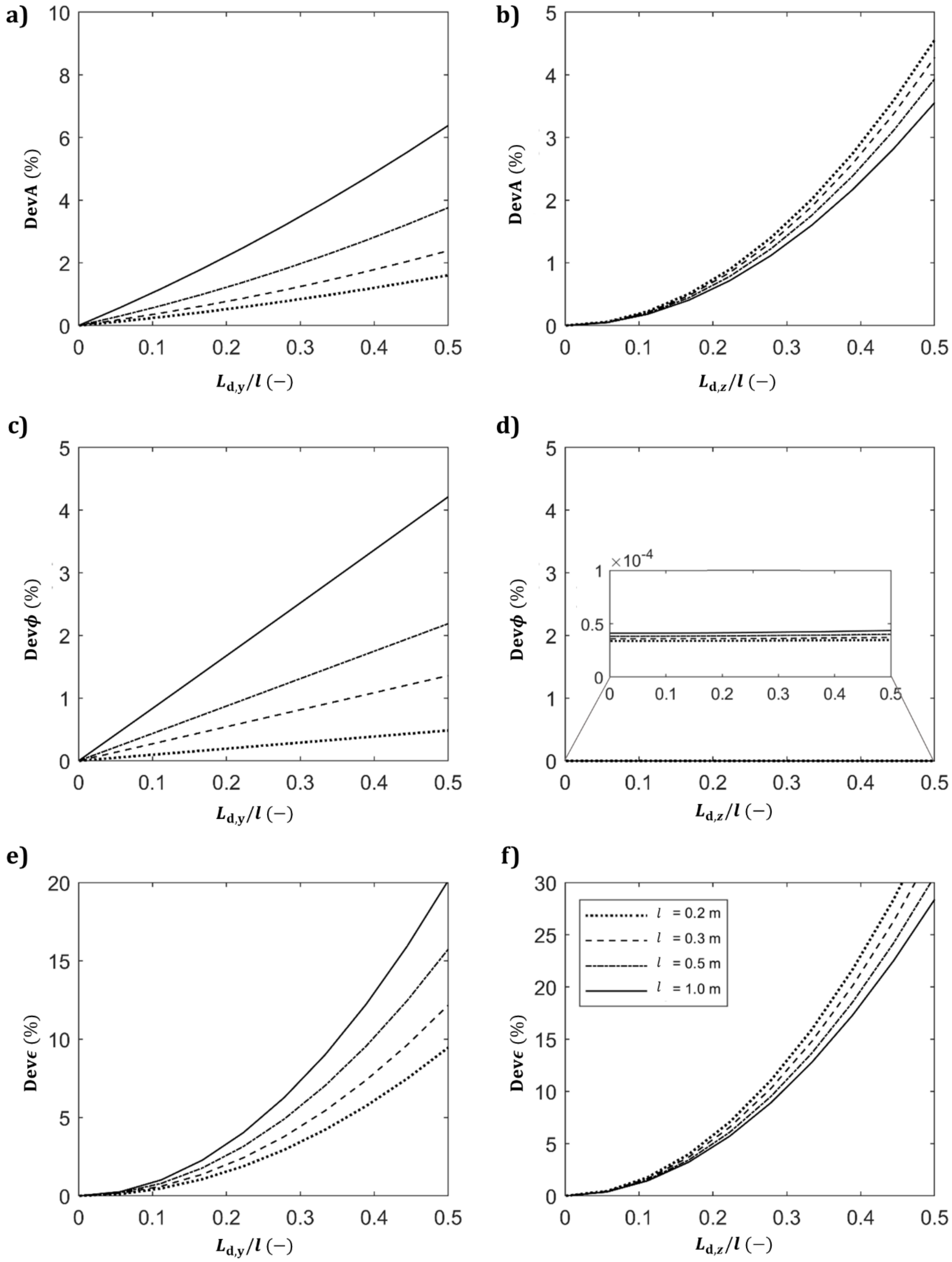

Figure 5. Deviations on (a-b) amplitude, (c-d) phase and (e-f) average values of the gas holdup wave, as a function of detector width and height normalized by the length of the radiation beam in the process space ($H_1 = -0.3669\ \mathrm{m^{-1}}$, $H_2 = 1.9502\ \mathrm{m^{-1}}$, $F/S = 8 \cdot 10^5\ \mathrm{m^{-2}}$, $A_{\epsilon,0}\mu_\mathrm{L} = 0.1\ \mathrm{m^{-1}}$, $L = 0.4\ \mathrm{m}$, $a = 0.3\ \mathrm{m}$).

Other examples for different values of H_1 and H_2 are reported in the **Supplementary Material S3**. The results show that the detector size has only a marginal influence on amplitude, phase and average value of the measured gas holdup wave. Thus, larger detectors (or combining several smaller ones) are recommended to reduce the total measurement time. It should be kept in mind, however, that for large detectors the deviation on the average holdup value might be non-negligible (see **Figure 5e,f**). The average holdup is linked with the bubble swarm velocity via $u_{\mathrm{G}}^{*} = u_{\mathrm{G}}/\bar{\epsilon}$, and a deviation on the bubble swarm velocity causes an additional deviation on the obtained axial gas dispersion coefficient, which is not considered here. This deviation has been analysed by Marchini et al. [4].

6. Impact of a frequency mismatch on measured amplitude and phase

When quartz-controlled timers are used in the measurement system, no relevant shift is expected between the sampling and modulation frequencies. However, to highlight the importance of correct synchronization the impact of a frequency shift is addressed here.

6.1 Quantification of the impact of a frequency mismatch on measured amplitude and phase

The deviation caused by a mismatch between the sampling and modulation frequencies is quantified modifying the algorithm proposed in Section 3. In this case, the real modulation and sampling frequencies f^* and f_{s}^*, respectively, are used to simulate the count data set sampled by the detector. In order to quantify the deviation, this obtained data set is then wrongly ensemble-averaged based on the expected number of intervals per modulation period n_{s}. Defining

$$\mathrm{Dev}n_{\mathrm{s}} = \frac{n_{\mathrm{s}}^{*} - n_{\mathrm{s}}}{n_{\mathrm{s}}}, \quad (31)$$

where $n_s^* = f_{\mathrm{s}}^*/f^*$, **Figure 6** reports an example of the impact of this frequency mismatch on the determined amplitude and phase in terms of Dev$A$ and Devϕ, as defined in Equations 28 and 29, respectively. For the sake of simplicity, signals free from other uncertainty sources are used here and f_s^*/f^* is assumed integer.

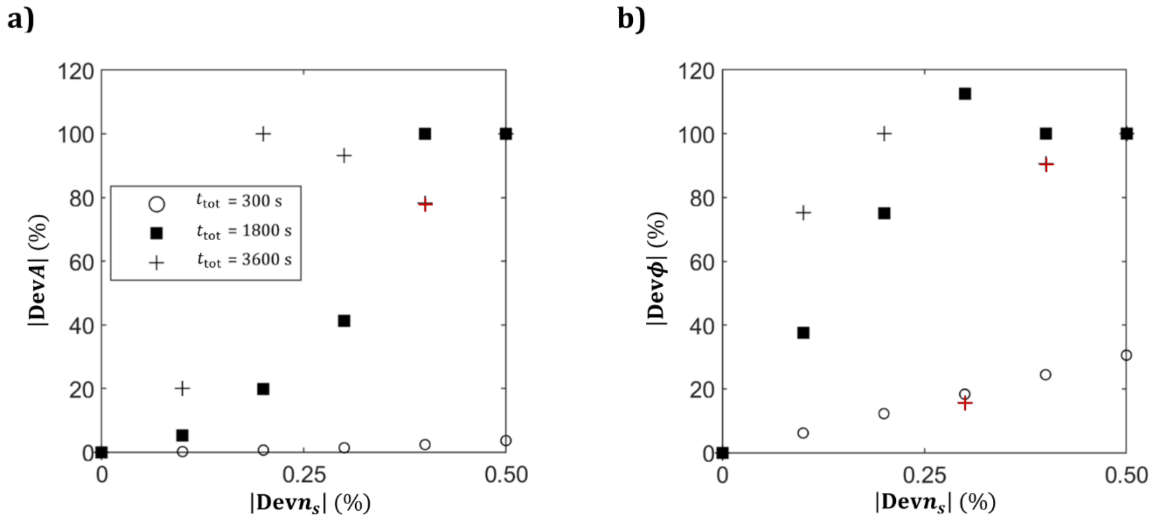

Figure 6. Impact of an unexpected deviation in the number of intervals per modulation period on amplitude and phase of the gas holdup wave (for $A = 0.15$, $\phi = 1.5$ rad, $K_1/(t_{\text{tot}}f) = 19.9\ \text{s}^{-1}$, $K_2 = 0.1$). |Dev$A$| and |Devϕ| generally increase with |Devn_s|. Points deviating from this trend are highlighted in red.

The impact of the frequency shift on the ensemble-averaged signal increases with the total scanning time and with the shift magnitude, reaching 100%. The few points deviating from the main trend in **Figure 6** (highlighted in red) are due to the periodicity of the cosine function or due to the inadequacy of the fitting function, as amplitudes approach zero. **Figure 6** shows that even a minor undetected change can cause the failure of the ensemble-averaging approach, especially for long total scanning times. An analytic prediction of the deviation caused in such a scenario is provided in the **Supplementary Material S4**.

6.2 Determining the modulation frequency from available detector data

If the modulation frequency is not known, it can be determined employing a discrete Fourier transform to the detector data. This, however, introduces an uncertainty in the determined frequency, which is quantified in this subsection. The maximum uncertainty of the determined frequency corresponds to the resolution of the frequency vector of the discrete Fourier transform equal to

$$\Delta f = \frac{1}{t_{\mathrm{tot}}}. \qquad 32$$

Based on Equation 31, the resolution of the Fourier transform causes a maximum deviation of n_{s} for given sampling frequency and total scanning time given by

$$\mathrm{Dev}n_{\mathrm{s}} = \frac{1}{t_{\mathrm{tot}} f_{\mathrm{s}}} n_{\mathrm{s}}^{*}. \qquad 33$$

For small deviation values

$$\mathrm{Dev}n_{\mathrm{s}} \cong \frac{1}{t_{\mathrm{tot}} f_{\mathrm{s}}} n_{\mathrm{s}}. \qquad 34$$

Therefore, the deviation caused by the limited resolution of the fast Fourier transform decreases increasing $t_{\mathrm{tot}} f_{\mathrm{s}}$ and increases linearly with n_{s}.

Figure 7 shows examples of how the uncertainty of the determined frequency (defined as in Equation 31) changes with the sampling time and the number of intervals per period n_{s}.

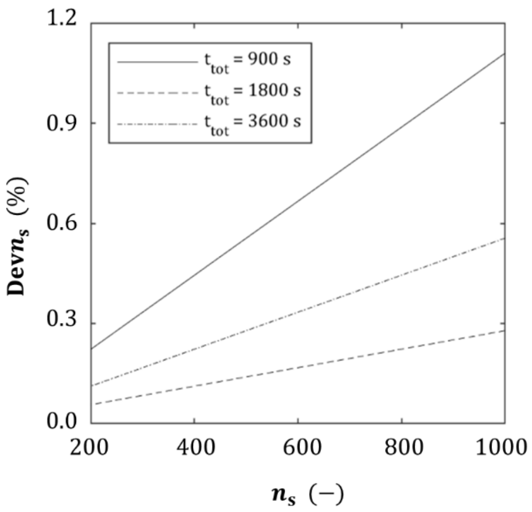

Figure 7. Deviation of the measured number of intervals per modulation period as a function of the expected value.

The shortcomings of the discrete fast Fourier transform are well-known in the literature and several techniques have been proposed to reduce the uncertainty of the determined frequency, for example by Kanatov et al. [6] and by Gasior and Gonzalez [7]. More specifically, the Gaussian interpolation of the frequency spectrum, proposed by Gasior and Gonzalez [7], is proved to reduce this uncertainty by up to three orders of magnitude. The application of these techniques allows reducing the uncertainty way more than increasing the total scanning time and should therefore be preferred.

Even a very small uncertainty of 0.1% on the sampling over the modulation frequency ratio can cause the failure of the approach (see **Figure 6**). Thus, care must be taken in selecting proper clocks for measurement system and signal detection. In addition, techniques to reduce the deviation due to the discrete nature of the fast Fourier transform should be implemented in the analysis, if the modulation frequency is not exactly known.

7. Uncertainties of the axial dispersion coefficient

When performing measurements, the average gas holdup value as well as the amplitude and phase of its wave at certain axial positions are obtained. This study quantifies the experimental uncertainties associated with these parameters, when gamma-ray densitometry is used as measurement technique. However, the experimental uncertainty for amplitude damping and phase-shift obtained from this study must be combined with the inherent uncertainty (related to the assumptions involved in Equations 4 and 5) that has been analyzed recently by Marchini et al. [4]. This allows obtaining the resulting uncertainty of the measured axial dispersion coefficient. For clarity, a scheme of contributions of inherent and experimental uncertainty is provided in **Figure 8**.

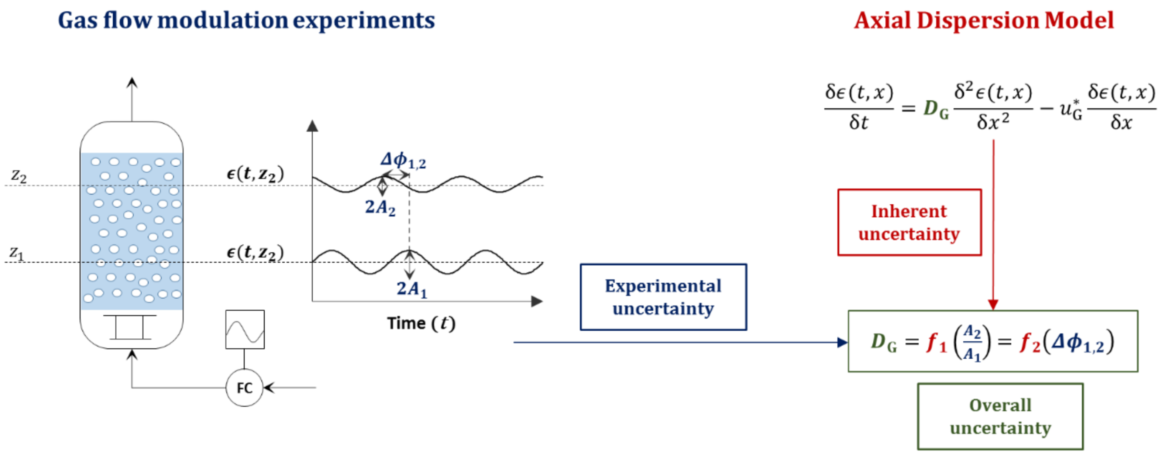

Figure 8. Scheme of experimental and inherent uncertainties influencing the overall uncertainty of the axial gas dispersion coefficient.

Marchini et al. [4] analyzed the derivative of the amplitude damping and phase-shift with respect to the axial dispersion coefficient. These are functions of the modulation and geometric parameters, the bubble rise velocity and the axial gas dispersion coefficient itself. Therefore, the same uncertainty of amplitude damping and phase-shift leads to different uncertainties on the axial gas dispersion coefficient considering different conditions.

As an example, **Figure 8** shows the sensitivity of the amplitude damping and phase-shift to the axial dispersion coefficient for different bubble rise velocities.

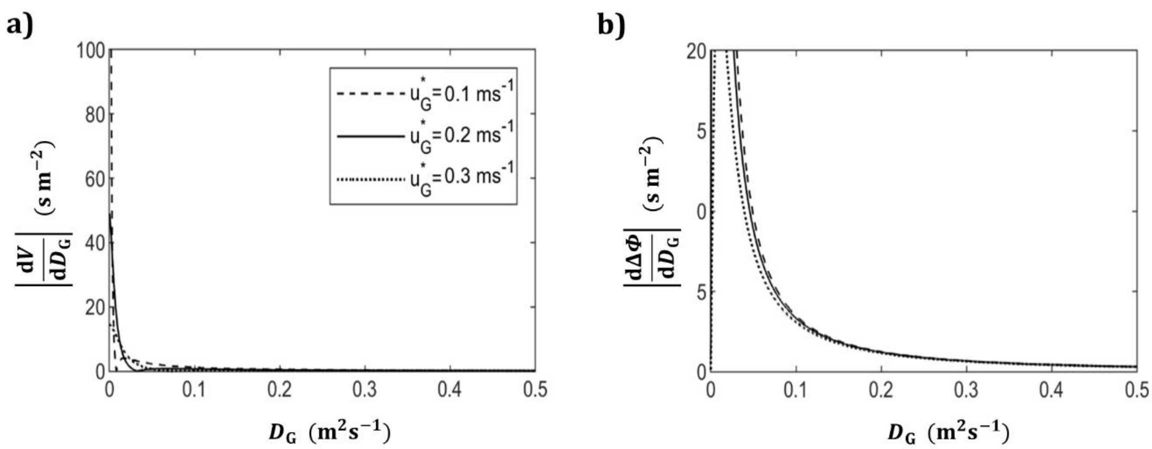

Figure 8. Sensitivity of (a) the amplitude damping and (b) the phase-shift to the axial gas dispersion coefficient obtained for different bubble rise velocities (f = 0.4 Hz, Δx =0.2 m).

8. Conclusions

We presented a study on the uncertainty of gamma-ray densitometry applied to the gas flow modulation technique and considered therefore the statistics of the photon counting process. The analyses shows that the measuring uncertainty, in principle, can be reduced by increasing the modulation amplitude, while modulation and sampling frequencies have no effects. However, this practice should be discouraged, since the modulation amplitude should always be kept below 0.15 as shown by Marchini et al. [4].

A reliable and systematic approach was proposed for quantifying the experimental uncertainty on the determined amplitude and phase of the gas holdup wave for various setup characteristics and operating conditions. The uncertainty connected with the detector size was quantified, too. In this way, in addition to increasing the total scanning time, the use of larger detectors (or the averaging of more adjacent detector elements) is a proper mean for reducing the uncertainty caused by the photon counting process. In this case, however, a well-centred alignment between source, column and detector is crucial.

It was further shown that the sampling frequency can be directly determined from the obtained data, applying a discrete fast Fourier transform. However, even an unexpected minimum deviation in the number of intervals per modulation period (i.e. in the frequency) can cause a failure of the ensemble-averaging approach. For this reason, extreme care should be taken in selecting the applied clocks and the limited resolution of the discrete Fourier transform should be kept in mind.

Altogether, the proposed algorithm and derived guidelines represent a powerful support for designing gamma densitometry measurement systems for future applications of the GFM (including characteristics of gamma-ray source and detector, geometry of the apparatus and needed performances of the clocks), as well as for selecting appropriate total scanning time, sampling frequency and modulation frequency.

9. Acknowledgement

This work was supported by the German Research Foundation (DFG) (HA 3088/18-1).

Nomenclature		**Unit**
a	Distance between source and column along the x axis for y=0 and z=0.	m
A	Amplitude of the sinusoidal gas holdup wave	
A_{ϵ}	Amplitude of the sinusoidal gas wave times average gas holdup.	
$A_{\epsilon,0}$	Initial amplitude of the sinusoidal gas wave times average gas holdup.	
Dev$A$	Deviation of the measured amplitude of the gas holdup wave	
c	Concentration of selected species in the studied phase	mol m^{-3}
C	Parameter used in Section 5, defined as $C = \sqrt{1+\left(\frac{x_{\mathrm{jk}}^{(2)}-x_{\mathrm{jk}}^{(1)}}{z_{\mathrm{jk}}^{(2)}-z_{\mathrm{jk}}^{(1)}}\right)^2+\left(\frac{y_{\mathrm{jk}}^{(2)}-y_{\mathrm{jk}}^{(1)}}{z_{\mathrm{jk}}^{(2)}-z_{\mathrm{jk}}^{(1)}}\right)^2}$	m
D	Axial gas dispersion coefficient	$m^2 s^{-1}$
e	Number of repetitions of a single experiment	
E	Time-domain Fourier transform of the gas holdup distribution	
f	Modulation frequency	Hz
Δf	Resolution of the frequency vector of the Fourier transform	Hz
f_{s}	Sampling frequency	Hz
F	Parameter used in Section 5, $F = \frac{\Phi S}{4\pi f_{\mathrm{s}}}$	
H_1	Parameter used in Section 5 defined as	m^{-1}

$$H_1 = \frac{u_G^*}{2D_G}\left[1 - \frac{1}{\sqrt{2}}\sqrt{1 + \sqrt{1 + \frac{16\omega^2 D_G^2}{{u_G^*}^4}}}\right]$$

H_2	Parameter used in Section 5 defined as	m^{-1}

$$\mathrm{H}_2 = -\frac{u_G^*}{D_G\sqrt{8}}\left[\sqrt{\left[\sqrt{1 + \frac{16\omega^2 D_G^2}{{u_G^*}^4}}\right] - 1}\right]$$

K_1	Parameter used in Section 4 defined as $K_1 = \frac{t_{\mathrm{tot}} f}{f_{\mathrm{s}}} \langle N_{\mathrm{G}} \rangle \exp\left(K_2\left(1 - \frac{1}{\bar{\epsilon}}\right)\right)$	cps
K_2	Parameter used in Section 4 defined as $K_2 = \mu_{\mathrm{L}} \bar{\epsilon} l$	
l	length of the radiation beam in the process space	m
L	Distance between source and detector	m
$L_{\mathrm{d,z}}$	Detector width	m
$L_{\mathrm{d,y}}$	Detector height	m
n	Scanning interval	
n_{s}	Number of scanning intervals per modulation period	
$\mathrm{Dev}n_{\mathrm{s}}$	Overall deviation of the determined number of intervals per modulation period	
n_{tot}	Total number of intervals in the total measurement time	
N	Number of counted photons	cps
$\langle N \rangle$	Expected number of counted photons	cps
$\langle N_{\mathrm{G}} \rangle$	Expected number of counts for the gas-filled column	cps
$\langle N_{\mathrm{GL}} \rangle$	Expected number of counts for the gas-liquid-filled column	cps
$\widetilde{N}_{\mathrm{GL}}$	Ensemble-averaged number of counts for the gas-liquid-filled column	cps
P	Probability	

$P^{(\mathrm{c})}$	Center of the detector element with coordinates $x^{(\mathrm{c})}, y^{(\mathrm{c})}, z^{(\mathrm{c})}$	
$P^{(1)}$	Point where the considered gamma-ray penetrates the column with coordinates $x^{(1)}, y^{(1)}, z^{(1)}$	
$P^{(2)}$	Point where the considered gamma-ray exits the column with coordinates $x^{(2)}, y^{(2)}, z^{(2)}$	
S	Detector surface ($S = L_{\mathrm{d,z}} L_{\mathrm{d,y}}$)	m^2
t	Time	s
t_{tot}	Total measurement time	s
u	Superficial velocity	ms^{-1}
u_{G}^{*}	Bubble rise velocity	ms^{-1}
V	Amplitude damping between two axial positions	
x, y	Coordinate axis with origin corresponding to the gamma-source	m
z	Axial coordinate of the bubble column (distance from the sparger)	m
Δz	Axial distance between the two measurement points	m

Greek letters

μ	Attenuation coefficient	m^{-1}
ϵ	Expected gas holdup wave	
$\tilde{\epsilon}$	Expected ensemble-averaged gas holdup wave	
$\bar{\epsilon}$	Expected gas holdup wave averaged over the entire measurement time	
$\mathrm{Dev}\bar{\epsilon}$	Deviation of the measured average gas holdup	
ϕ	Phase of the gas holdup wave	rad
$\Delta\phi$	Phase-shift in the gas holdup wave between the measurement points	rad
$\mathrm{Dev}\phi$	Deviation on the phase of the gas holdup wave	

Φ	Photon intensity	cps sr^{1}
ω	Angular modulation frequency	rad s^{-1}

Subscripts

i, j, w, k	Indexes
G	Gas phase
L	Liquid phase

Superscripts

j, i	Refers to detector element (j,i)
$*$	Measured value (in contrast to the expected value)

References

[1] U. Hampel, Anordnung und Verfahren zur Dispersionsmessung sowie Mehrphasenapparat mit einer solchen Anordnung. Patent DE 10 2014 118 649 B3 2015.12.24., 2015.

[2] M.V. Kantak, S.A. Shetty, B.G. Kelkar, Liquid-Phase Backmixing in Bubble-Column Reactors - a New Correlation, Chemical Engineering Communications 127 (1994) 23-34.

[3] F. Demaria, R.R. White, Transient Response Study of Gas Flowing through Irrigated Packing, Aiche Journal 6 (1960) 473-481.

[4] S. Marchini, M. Schubert, U. Hampel, Analysis of the effect of uncertainties in hydrodynamic parameters on the accuracy of the gas flow modulation technique for bubble columns, Chemical Engineering Jornal 434 (2022).

[5] A. Döß, M. Schubert, A. Bieberle, U. Hampel, Non-invasive determination of gas phase dispersion coefficients in bubble columns using periodic gas flow modulation, Chemical Engineering Science 171 (2017) 256-270.

[6] I. Kanatov, D. Kaplun, D. Butusov, V. Gulvanskii, A. Sinitca, One Technique to Enhance the Resolution of Discrete Fourier Transform, Electronics 8 (2019) 330.

[7] M. Gasior, J. Gonzalez, Improving FFT frequency measurement resolution by parabolic and gaussian interpolation, CERN-AB-Note-2004-021, 2004.